

# ERROR ESTIMATION INCLUDING POLLUTION ASSESSMENT FOR NONLINEAR FINITE ELEMENT ANALYSIS

Antonio HUERTA and Pedro DÍEZ

*Departament de Matemàtica Aplicada III  
E.T.S. Ingenieros de Caminos  
Universitat Politècnica de Catalunya  
E-08034 Barcelona, SPAIN*

---

## Abstract

A residual type error estimator for nonlinear finite element analysis is introduced. This error estimator solves local problems avoiding both the computation of the flux jumps and the associated flux splitting procedure. Pollution errors are taken into account by a feedback strategy, that is, an error estimate based on local computations is used as the input of the pollution analysis. This estimator is used in the frame of an adaptive procedure. Numerical examples show the estimator is able to drive adaptive procedures leading to likely good solutions. Moreover, one of the examples demonstrates that adaptive procedures are essential for complex highly nonlinear mechanical problems because they may discover secondary collapse mechanisms.

*Key words:* Finite Elements, Error estimation, Pollution errors, Adaptivity, Nonlinearity

---

## 1 Introduction

The use of finite elements for practical engineering problems requires adaptive computations. The scheme of a generic adaptive procedure is represented in Figure 1. Error estimation is a key ingredient in any adaptive procedure because the acceptability criteria are based on the error estimate. Moreover, the error estimate is essential to relate the output of the previous computation with the requirements of the next mesh.

Error estimators for linear problems are standard and perform well [26,27]. Error estimators may be classified mainly into two groups: 1) flux projection or ZZ-like [32] error estimators and 2) residual type error estimators [7,1,17], see also [31] for a study of their relationship. Many nonlinear generalizations have been defined from linear estimators. Nevertheless, most of them lose the sound theoretical basis of the linear counterpart because they are based on properties that stand only for linear problems [8,14,15,18,22,29,33].

Here, the generalization of a residual estimator [11] to nonlinear problems is presented. The performance of this estimator does not depend on superconvergence properties, which have only been proved for linear problems. Moreover, the presented approach can be applied to general unstructured meshes with different element types (for instance, triangles and quadrilaterals). Consequently, assuming that a sound equation for the error is provided, this estimator is easily applied to nonlinear problems. Here the nonlinear error equation is linearized by means of a tangent Taylor expansion. Moreover, using this estimator, a method for assessing pollution errors is readily available both for linear and nonlinear problems.

It is important to notice that, generally, a distinction is made between error estimators and error indicators. This distinction requires a definition which has not been yet universally stated. In this context, error indicators are based on heuristic considerations while error estimators approximate a measure of the actual error in a given norm. Here, a tool for assessing the error measured in the energy norm is proposed. The obtained approximation to the error is asymptotically exact, that is, tends to the actual error if the element size tends to zero, see also [2,3]. In that sense, this tool is an error estimator.

The remainder of the paper is structured as follows. Section 2 states the problem and introduces the notation. In section 3 the philosophy and the mechanism of the linear error estimator introduced in [11] is described. The presentation of the linear estimator is oriented to easily extend it to the nonlinear case, this extension is presented in section 4. In section 5 several numerical examples of adaptive computations using this estimator are presented. These examples demonstrate the ability of the introduced estimator to deal with highly nonlinear mechanical problems. Finally, section 6 includes some concluding remarks.

## 2 Model problem

Let  $\Omega$  be a bounded domain in  $\mathbb{R}^2$  with a smooth boundary  $\partial\Omega$ . The boundary  $\partial\Omega$  is divided into two parts  $\Gamma_D$  and  $\Gamma_N$  such that  $\partial\Omega = \bar{\Gamma}_D \cup \bar{\Gamma}_N$  and

$\Gamma_D \cap \Gamma_N = \emptyset$ . The standard Sobolev space

$$H_{\Gamma_D}^1(\Omega) := \{v \in H^1(\Omega) \text{ such that } v = 0 \text{ on } \Gamma_D\}$$

is introduced as the natural space containing the concerned functions.

The unknown function  $u$  is the solution of the following boundary-value problem:

Find  $u$  in  $H_{\Gamma_D}^1(\Omega)$  such that

$$a(u, v) = l(v) \text{ for all } v \in H_{\Gamma_D}^1(\Omega), \quad (1)$$

where the forms  $a(\cdot, \cdot)$  and  $l(\cdot)$  are defined in  $H_{\Gamma_D}^1(\Omega) \times H_{\Gamma_D}^1(\Omega)$  and  $H_{\Gamma_D}^1(\Omega)$ , respectively.

**Remark 1** *Although  $u$  belongs to  $H_{\Gamma_D}^1(\Omega)$  (that is,  $u = 0$  on  $\Gamma_D$ ) the Dirichlet boundary conditions on  $\Gamma_D$  in the original boundary value problem may be non-homogeneous.*

The form  $a(\cdot, \cdot)$  is linear with respect to its second argument. In linear problems,  $a(\cdot, \cdot)$  is bilinear. In particular, for second order linear self-adjoint problems,  $a(\cdot, \cdot)$  is bilinear and symmetric. Moreover, in many problems (for instance, in linear elasticity),  $a(\cdot, \cdot)$  is also positive definite and, hence, it is a scalar product.

The Galerkin finite element method provides an approximation  $u_h$  to  $u$ , lying in a finite-dimensional space  $V_h \subset H_{\Gamma_D}^1(\Omega)$  and verifying

$$a(u_h, v_h) = l(v_h) \text{ for all } v_h \in V_h. \quad (2)$$

The finite-dimensional space  $V_h$  is associated with a finite element mesh of characteristic size  $h$ . The elements of this mesh are denoted by  $\Omega_k$ ,  $k = 1, 2, \dots$  and it is assumed that  $\bar{\Omega} = \bigcup_k \bar{\Omega}_k$ .

The goal of a posteriori error estimation is to assess the accuracy of the approximate solution  $u_h$ . This is done analyzing the error  $e := u - u_h$  and estimating both global and local measures of the error. Local measures are used to describe the spatial distribution of the error and the global measure, which is employed to verify the acceptability criterion, is obtained summing up the local contributions.

Thus, a norm to measure the error must be defined. One of the most popular options (in the linear case) is the energy norm induced by  $a(\cdot, \cdot)$ :

$$\|e\| := [a(e, e)]^{1/2}. \quad (3)$$

The reasons for choosing  $\|\cdot\|$  are: it has physical meaning, it is equivalent to standard Sobolev norms and it can be easily restricted in order to obtain associated local norms.

In the following, the restriction of  $\|\cdot\|$  to the element  $\Omega_k$  ( $k = 1, 2, \dots$ ) of the mesh is denoted by  $\|\cdot\|_k$ . The value of  $\|e\|_k$  in each element must be estimated in order to describe the spatial distribution of  $e$ . A suitable extension of the linear estimator maintaining most of its properties is defined for the nonlinear case.

### 3 Linear a posteriori error estimation

Typically, for linear elasticity, linear heat diffusion, etc,  $a(\cdot, \cdot)$  is a scalar product. Then  $u_h$  is the projection of  $u$  on  $V_h$  and the error  $e = u - u_h$  is orthogonal to  $V_h$  in the sense of  $a(\cdot, \cdot)$ . As previously said, the objective of this error estimator is to assess both a global value of the error and its spatial distribution.

Assuming that  $a(\cdot, \cdot)$  is bilinear, Eq. (1) can be easily rearranged to obtain a weak equation for the error. The error  $e$  is the element in  $H_{\Gamma_D}^1(\Omega)$  that verifies

$$a(e, v) = l(v) - a(u_h, v) \text{ for all } v \in H_{\Gamma_D}^1(\Omega). \quad (4)$$

Note that the right-hand-side of Eq. (4) is a residual term which accounts for the non-verification of Eq. (1).

#### 3.1 The reference error

The error  $e$  is unknown and it is impossible to obtain its exact value. Thus, the only attainable goal is to obtain an approximation to  $e$ , say  $e_{\tilde{h}}$ . This approximation to the error can be easily defined from a new approximation to  $u$ , say  $u_{\tilde{h}}$ , more accurate than  $u_h$ . For instance,  $u_{\tilde{h}}$  may be a finite element approximation associated with a finer mesh of characteristic size  $\tilde{h}$  ( $\tilde{h} \ll h$ ). The associated interpolation space  $V_{\tilde{h}}$  is much richer than  $V_h$ . Then  $u_{\tilde{h}}$  is much more precise than  $u_h$  and, therefore,  $e_{\tilde{h}} := u_{\tilde{h}} - u_h$  is a good approximation of  $e$ . This is formally shown in [21] as a consequence of the a priori convergence analysis of the finite element method.

**Remark 2** *The a priori error analysis of the finite element method gives error bounds like (see [16])*

$$\|e\| = \|u - u_h\| \leq Ch^p \quad \text{and} \quad \|u - u_{\tilde{h}}\| \leq C\tilde{h}^p, \quad (5)$$

where  $p$  stands for the degree of the interpolating polynomial. Applying Richardson extrapolation and the orthogonality between  $e_{\tilde{h}}$  and  $u - u_{\tilde{h}}$ , it can be shown that

$$\|u - u_{\tilde{h}}\| = \|e_{\tilde{h}}\| \simeq \left[ 1 - \left( \frac{\tilde{h}}{h} \right)^{2p} \right]^{1/2} \|e\|. \quad (6)$$

That is, if  $\tilde{h}$  is one fourth of  $h$  and  $p$  is one, the reference error,  $e_{\tilde{h}}$ , is 97% of the actual error  $e$ .

In the following, the finer mesh of element size  $\tilde{h}$  is denoted as the reference mesh, as well as the associated solution,  $u_{\tilde{h}}$ , is the reference solution and  $e_{\tilde{h}}$  is the reference error. Note that the discretization can be enriched using different strategies: instead of the  $h$ -refinement approach (reduce the element size), the  $p$ -refinement approach (increase the degree of the interpolation polynomial) can also be used to increase the accuracy of the interpolation and define a reference solution. Here, for the simplicity of the presentation, only the  $h$ -refinement approach is presented.

In fact, computing  $u_{\tilde{h}}$  and then obtaining  $e_{\tilde{h}}$  is equivalent to directly solving the error equation (4) using the finer mesh. That is, solving Eq. (1) using  $V_{\tilde{h}}$  is equivalent to solving Eq. (4) using the same interpolation space. Thus,  $e_{\tilde{h}}$  is the element of  $V_{\tilde{h}}$  that verifies

$$a(e_{\tilde{h}}, v_{\tilde{h}}) = l(v_{\tilde{h}}) - a(u_h, v_{\tilde{h}}) \text{ for all } v_{\tilde{h}} \in V_{\tilde{h}}. \quad (7)$$

Nevertheless, the standard computation of  $e_{\tilde{h}}$  must be avoided due to its prohibitive computational cost: the refined mesh generating  $V_{\tilde{h}}$  has a number of degrees of freedom much larger than the original mesh and, therefore, the cost of computing  $e_{\tilde{h}}$  is usually prohibitive.

In the remainder of this section a method for approximating  $e_{\tilde{h}}$  by low cost local computations is presented. This method is split in two phases. First, a simple residual problem is solved inside each element and an interior estimate is obtained. Second, a new family of simple problems is considered and the interior estimate is complemented adding a new contribution. The first phase is called interior estimation and the latter is called patch estimation.

### 3.2 Interior estimation

Solving the global reference problem, see Eq. (7), implies the resolution of a very large system of equations with a prohibitive computational cost. In order

to avoid unaffordable computations, the error estimation must be performed solving local problems. In fact, standard residual-type error estimators solve elementary problems because the natural partition of the domain is the set of elements of the “coarse” computational mesh,  $\Omega_k$ ,  $k = 1, 2, \dots$

Here, each element  $\Omega_k$  is discretized by an elementary submesh built from a discretization of the reference element and mapped into  $\Omega_k$ , see Figure 2. Then, the reference mesh is constructed by the assembly of the elementary submeshes discretizing each element, see Figure 3. That is, each element  $\Omega_k$  of the mesh is associated with a local interpolation space  $V_{\tilde{h},k}$ , induced by the corresponding elementary submesh. In fact, this space  $V_{\tilde{h},k}$  is a finite-dimensional subset of  $H^1(\Omega_k)$ . Notice that the functional space  $\bigoplus_k V_{\tilde{h},k}$  does not coincide with  $V_{\tilde{h}}$  because the former includes functions which are discontinuous along the element edges.

Then, the elementary submeshes can be used to solve the error equation, see Eq (4), on each element  $\Omega_k$  of the original mesh. However, the solution of such problems requires proper boundary conditions for the error. Most of residual type error estimators (see [7,1,17]), solve Eq. (4) prescribing the flux around each element  $\Omega_k$ , that is, solving pure Neumann problems. The prescribed values of error fluxes are found splitting the jump of the fluxes of  $u_h$  across the element edges. The computation of the flux jumps across the edges is expensive. The splitting procedure usually equilibrates the fluxes around the element and, therefore, is generally involved.

In this work, the elementary problems are solved in a straightforward manner imposing homogeneous Dirichlet conditions for the error, along the boundary of each element  $\Omega_k$ , see [11]. That is, the approximation to the error is prescribed to zero in all the boundary nodes of the elementary submesh. In other words, the local problem is solved in the interpolation space  $V_{\tilde{h},k,0} := V_{\tilde{h},k} \cap H_0^1(\Omega_k)$ , where  $H_0^1(\Omega_k) := \{v \in H^1(\Omega_k) \text{ such that } v = 0 \text{ in } \partial\Omega_k \setminus (\partial\Omega_k \cap \Gamma_N)\}$ . The solution of this local problem is the function  $\varepsilon_k$  verifying:

$$a(\varepsilon_k, v_{\tilde{h}}) = l(v_{\tilde{h}}) - a(u_h, v_{\tilde{h}}) \text{ for all } v_{\tilde{h}} \in V_{\tilde{h},k,0}. \quad (8)$$

**Remark 3** According to the definition of  $V_{\tilde{h},k,0}$ , the error is set equal to zero on  $g_D$  (which is a true condition because  $u_h$  is equal to  $u$  on  $\Gamma_D$ , up to the accuracy of the discretization) but also on the interior element boundaries (where it is unknown). That is, the error is artificially set to zero along the (interior) interelement boundaries. Notice that the flux of the error can be computed on  $\Gamma_N$  and this condition is implicitly imposed in Eq. (8) via the residual right-hand-side term.

**Remark 4** Assuming that  $a(\cdot, \cdot)$  is a scalar product,  $\varepsilon_k$  is the projection of  $e_{\tilde{h}}$  on  $V_{\tilde{h},k,0}$ .

This discrete local problem leads to a system of equations

$$\mathbf{K}_{\tilde{h},k}^e \boldsymbol{\varepsilon}_k = \mathbf{r}_k^e, \quad (9)$$

where  $\mathbf{K}_{\tilde{h},k}^e$  is the stiffness matrix resulting of discretizing  $a(\cdot, \cdot)$  in a basis of  $V_{\tilde{h},k,0}$  which is the set of the standard finite element interpolation functions associated with the elementary submesh. The column vector  $\mathbf{r}_k^e$  results of discretizing the residual form  $l(\cdot) - a(u_h, \cdot)$ , see Eq. (8), in the same basis. The vector  $\boldsymbol{\varepsilon}_k$  is the expression of  $\varepsilon_k$  in the chosen basis. The local energy norm of the interior estimate  $\varepsilon_k$  can be directly computed since

$$\|\varepsilon_k\|^2 = a(\varepsilon_k, \varepsilon_k) = \boldsymbol{\varepsilon}_k^T \mathbf{K}_{\tilde{h},k}^e \boldsymbol{\varepsilon}_k = \boldsymbol{\varepsilon}_k^T \mathbf{r}_k^e. \quad (10)$$

Thus, since  $\varepsilon_k$  has its support in  $\Omega_k$ , local and global norms are equal:  $\|\varepsilon_k\| = \|\varepsilon_k\|_k$ . Recall that the local restriction of the norm  $\|\cdot\|$  to the element  $\Omega_k$ ,  $\|\cdot\|_k$ , is used to obtain elementary measures of the error and to describe the error distribution.

Once the elementary problems are solved, the local interior estimates can be assembled to build up a global estimate  $\varepsilon$  having values in the whole domain  $\Omega$ ,

$$\varepsilon = \sum_k \varepsilon_k, \quad (11)$$

where, for a proper definition of the previous sum, the local functions  $\varepsilon_k$  are continuously extended in the whole  $\Omega$ . The interior estimates  $\varepsilon_k$  and  $\varepsilon_{k'}$  associated with different elements ( $k \neq k'$ ) are orthogonal because they have disjoint supports ( $\Omega_k \cap \Omega_{k'} = \emptyset$ ). Then, Pythagoras theorem holds and the norm of  $\varepsilon$  can be easily computed:

$$\|\varepsilon\|^2 = \sum_k \|\varepsilon_k\|^2. \quad (12)$$

Both local,  $\varepsilon_k$ , and global,  $\varepsilon$ , interior estimates are projections of  $e$  (and also of  $e_{\tilde{h}}$ ) on the respective subspaces  $V_{\tilde{h},k,0}$  and  $\bigoplus_k V_{\tilde{h},k,0}$ , which are included in  $V_{\tilde{h}}$  (the inclusion in  $V_{\tilde{h}}$  is verified because of the homogeneous Dirichlet boundary condition, which preserves global continuity: note that  $V_{\tilde{h},k,0} \subset V_{\tilde{h}}$  and  $\bigoplus_k V_{\tilde{h},k,0} \subset V_{\tilde{h}}$ ). Consequently the norms of the interior estimates are lower bounds of the actual and reference errors:

$$\|\varepsilon\| \leq \|e_{\tilde{h}}\| \leq \|e\| \quad \text{and} \quad \|\varepsilon_k\|_k = \|\varepsilon\|_k \leq \|e_{\tilde{h}}\|_k \leq \|e\|_k. \quad (13)$$

The choice of the artificial boundary condition may imply that  $\|\varepsilon\| \ll \|e\|$ .

This is a consequence of forcing the approximation  $\varepsilon$  to be zero along the interelement boundaries. Since the reference error  $e_{\tilde{h}}$  is generally nonzero in all these points,  $\varepsilon$  may be a poor approximation to  $e_{\tilde{h}}$ . In other words, interior residuals are considered in the right-hand-side term of Eq. (8) but the information contained in the flux jumps is ignored.

### 3.3 Patch estimation and complete estimate

Once the interior estimate is computed a new contribution must be added in order to account for the flux jumps. This is equivalent to improve the error estimation by adding nonzero values in the interelement boundaries. In this section, this is done following the same idea of the interior estimation, precluding the direct computation of flux jumps and avoiding the flux splitting procedure.

The interior estimate is based on solving local problems within the elements  $\Omega_k$ ,  $k = 1, 2, \dots$ . But other partitions can also be used: let us consider a new family of disjoint subdomains  $(\Lambda_l, l = 1, 2, \dots)$  covering  $\Omega$ . Each one of these subdomains  $\Lambda_l$  overlaps a few number of elements. Moreover, these subdomains include the interelement boundaries. In order to simplify the exposition, in the following, the subdomains  $\Lambda_l$  are called patches. Using the elementary submeshes of Figure 2, the most natural choice for patch subdomains is to associate them with the nodes of the mesh: each patch is associated with a node and includes a fourth of every element sharing that node (see Figure 4 for an illustration and [11] for a detailed presentation).

Each patch submesh induces an interpolation subspace  $U_{\tilde{h},l}$ . The space  $U_{\tilde{h},l}$  is associated with  $\Lambda_l$  in the same way that  $V_{\tilde{h},k}$  is associated with  $\Omega_k$ . In order to impose local boundary conditions  $e_{\tilde{h}}$  is approximated in  $U_{\tilde{h},l,0} := U_{\tilde{h},l} \cap H_0^1(\Lambda_l)$ , where  $H_0^1(\Lambda_l) := \{v \in H^1(\Lambda_l) \text{ such that } v = 0 \text{ in } \partial\Lambda_l \setminus (\partial\Lambda_l \cap \Gamma_N)\}$ . Thus, over each patch  $\Lambda_l$ , a new local estimate  $\eta_l$ , is computed such that it belongs to  $U_{\tilde{h},l,0}$  and verifies

$$a(\eta_l, v_{\tilde{h}}) = l(v_{\tilde{h}}) - a(u_h, v_{\tilde{h}}) \text{ for all } v_{\tilde{h}} \in U_{\tilde{h},l,0}. \quad (14)$$

Eq. (14) can also be written in a matrix form analogous to Eq. (9)

$$\mathbf{K}_{\tilde{h},l}^p \boldsymbol{\eta}_l = \mathbf{r}_l^p, \quad (15)$$

where matrix  $\mathbf{K}_{\tilde{h},l}^p$  and vectors  $\boldsymbol{\eta}_l$  and  $\mathbf{r}_l^p$  are the expressions of  $a(\cdot, \cdot)$ ,  $\eta_l$  and  $l(\cdot) - a(u_h, \cdot)$  in a basis of  $U_{\tilde{h},l,0}$ . Thus, the norm of  $\eta_l$  can be easily computed



as

$$\|\eta_l\|^2 = \boldsymbol{\eta}_l^T \mathbf{r}_l^p \quad (16)$$

and, again, the local estimates can be assembled to build up a global estimate having values in the whole domain  $\Omega$ :

$$\eta = \sum_l \eta_l. \quad (17)$$

The norm of  $\eta$  can be easily computed, due to the orthogonality of the different spaces  $U_{\tilde{h},l,0}$  (patches are disjoint):

$$\|\eta\|^2 = \sum_l \|\eta_l\|^2. \quad (18)$$

Nevertheless, the norm of  $\eta$  cannot be directly added to the norm of the interior estimate  $\varepsilon$  because  $\eta$  and  $\varepsilon$  are not orthogonal. In order to easily add the two contributions,  $\eta$  is forced to be orthogonal to  $\varepsilon$ . That is, an additional condition to each  $\eta_l$  is imposed in Eq. (14). This orthogonality condition is written

$$a(\varepsilon, \eta_l) = 0, \quad (19)$$

and can also be seen as a linear restriction to vector  $\boldsymbol{\eta}_l$  in Eq. (15):

$$\boldsymbol{\varepsilon}^T \mathbf{K}_{\tilde{h},l}^p \boldsymbol{\eta}_l = 0. \quad (20)$$

**Remark 5** *The orthogonality condition of Eq. (20) is a linear restriction and can be imposed either a priori, modifying the system of equations (15), or a posteriori, solving the original Eq. (15) and modifying the result. The first option seems to be more natural since it corresponds to projecting on a restricted space and it is easily implemented using the Lagrange multiplier technique. The latter option consists on freely projecting  $e_{\tilde{h}}$  on  $U_{\tilde{h},l,0}$ , that is, solving Eq. (15), and then subtracting the projection of the result on  $\text{span} \langle \varepsilon \rangle$ . Thus, a free projection, say  $\eta_l^{\text{free}}$ , is computed first and, then, the restricted one,  $\eta_l$  is obtained as*

$$\eta_l = \eta_l^{\text{free}} - \frac{a(\eta_l^{\text{free}}, \varepsilon)}{a(\varepsilon, \varepsilon)} \varepsilon.$$

Thus,  $\eta$  is computed using the orthogonality condition of Eq. (19) or Eq. (20) and the patch estimate  $\eta$  can be added to the former interior estimate  $\varepsilon$  to

build up an approximation to the reference error having values in the whole domain  $\Omega$ :

$$e_{\tilde{h}} \simeq e_L := \varepsilon + \eta. \quad (21)$$

This estimate is denoted by  $e_L$  because it is obtained performing only local computations. The global and local norms of  $e_L$  can be easily computed:

$$\|e_L\|^2 = \|\varepsilon\|^2 + \|\eta\|^2 \quad (22)$$

and

$$\|e_L\|_k^2 = \|\varepsilon\|_k^2 + \|\eta\|_k^2 = \|\varepsilon_k\|^2 + \sum_l \|\eta_l\|_k^2. \quad (23)$$

Notice that in the sum of Eq. (23) subscript  $l$  ranges only the values such that  $\Lambda_l$  overlaps  $\Omega_k$ , that is,  $\Lambda_l \cap \Omega_k \neq \emptyset$ , see [11].

The global measure of the local estimate maintains the lower bound properties, that is,  $\|e_L\| \leq \|e_{\tilde{h}}\|$ . Moreover, taking into account the contribution of the patches, the complete estimate  $\|e_L\|$  is a quite good approximation of the reference error  $\|e_{\tilde{h}}\|$  (and also of the actual error  $\|e\|$ ). An analysis of the efficiency of this estimator can be found in [12].

### 3.4 Assessment of the pollution error

The error estimation strategy presented above gives an estimate  $e_L$  based on local computations. Consequently, the error effects associated with the pollution [28] are ignored. The pollution error is contained in the forgotten global part  $e_G := e_{\tilde{h}} - e_L$ . In this section, a method for approximating  $e_G$  is presented that allows to capture the associated pollution effects. Babuška and coworkers, see [4–6], introduced a pollution estimate which is mainly related with Green functions. In a Boundary Value Problem, the Green functions describe the interaction between different points of the domain, consequently the pollution that affects some point can be assessed by estimating the error in the approximation of the associated Green function. Here, the approach is completely different: the pollution is taken into account because the estimation of the global part of the error,  $e_G$ , is carried out performing a global computation.

Replacing the definition of  $e_G$  in Eq. (4), it can be easily found that  $e_G$  is the element of  $V_{\tilde{h}}$  verifying

$$a(e_G, v_{\tilde{h}}) = l(v_{\tilde{h}}) - a(u_h, v_{\tilde{h}}) - a(e_L, v_{\tilde{h}}) \text{ for all } v_{\tilde{h}} \in V_{\tilde{h}}. \quad (24)$$

Again, solving Eq. (24) is computationally unaffordable because it is a global problem defined on the reference mesh. However,  $e_G$  can be approximated using the standard Galerkin finite element method with the original mesh generating  $V_h$ . That is,  $e_G$  is approximated by  $e_G^*$  in  $V_h$  such that

$$a(e_G^*, v_h) = l(v_h) - a(u_h, v_h) - a(e_L, v_h) \text{ for all } v_h \in V_h. \quad (25)$$

Using Eq. (2), a simpler version of Eq. (25) is found:

$$a(e_G^*, v_h) = -a(e_L, v_h). \text{ for all } v_h \in V_h. \quad (26)$$

The resolution implies a linear system of equations having the same matrix as Eq. (2). Then, if a direct solver was employed in Eq. (2), the main cost of solving Eq. (26) is to evaluate the right-hand-side term.

**Remark 6**  $e_L$  is the projection of  $e_{\tilde{h}}$  on a subspace included in  $V_{\tilde{h}}$ , more precisely, this subspace is

$$\left\{ \bigoplus_l U_{\tilde{h},l,0} \right\} + \text{span} \langle \varepsilon \rangle .$$

Consequently,  $e_G$  is orthogonal to  $e_L$  and

$$\|e_{\tilde{h}}\|^2 = \|e_L\|^2 + \|e_G\|^2 \geq \|e_L\|^2 + \|e_G^*\|^2$$

because  $\|e_G\| \geq \|e_G^*\|$ . That is, the error estimate including the contribution on  $e_G^*$  maintains the lower bound properties.

## 4 Nonlinear generalization

### *Fully nonlinear problem*

If, the problem is nonlinear, the first argument of the form  $a(\cdot, \cdot)$  is nonlinear, that is,

$$a(e + u_h, v) \neq a(e, v) + a(u_h, v). \quad (27)$$

This case includes general sources of nonlinearity. For instance, in mechanical problems, both material (associated with the constitutive model) and geometric nonlinearities are accounted for.

Consequently, the linear error equation Eq. (4), does not stand anymore. In fact, the only available equation for the error is found re-writing Eq. (1):

$$a(e + u_h, v) = l(v) \text{ for all } v \in V. \quad (28)$$

This equation is associated with a reference error  $e_{\tilde{h}}$  in  $V_{\tilde{h}}$  which could be computed using the reference mesh:

$$a(e_{\tilde{h}} + u_h, v_{\tilde{h}}) = l(v_{\tilde{h}}) \text{ for all } v_{\tilde{h}} \in V_{\tilde{h}}, \quad (29)$$

This is unaffordable from a computational point of view, specially for nonlinear problems. A method for approximating  $e_{\tilde{h}}$  by local inexpensive computations is introduced in [13] for mechanical problems. This method follows the main philosophy of the linear estimator presented in the previous section. Thus, firstly  $e_{\tilde{h}}$  is approximated solving elementary problems subject to homogeneous Dirichlet-type boundary conditions (interior estimate) and, secondly, the estimate is completed by adding the contribution of a new set of approximations defined over a family of subdomains denoted as patches.

Nevertheless, often Eq. (29) can be simplified and an approximate linear equation for the error is obtained. This is very useful because once a linear error equation is found, the philosophy and the structure of the linear estimator presented in the previous section can be extended for nonlinear problems in a straightforward manner. This extension is presented in the remainder of this section.

### *Tangent approximation and nonlinear error estimation*

The error is assumed to be small compared with the solution. This stands also for the reference error, that is,  $\|e_{\tilde{h}}\| \ll \|u_h\|$ . Thus, the first argument of  $a(\cdot, \cdot)$ , which is a nonlinear function, can be properly approximated using a tangent expansion around  $u_h$ , see [9]:

$$a(e + u_h, v) \approx a(u_h, v) + a_T(u_h; e, v). \quad (30)$$

where  $a_T(u_h; \cdot, \cdot)$  is the linear approximation to  $a(\cdot, \cdot)$  around  $u_h$ .

Replacing Eq. (30) in Eq. (28), an approximation for the error equation is found:

$$a_T(u_h; e, v) = l(v) - a(u_h, v) \text{ for all } v \in H_{\Gamma_D}^1(\Omega). \quad (31)$$

Eq. (31) is linear and very similar to Eq. (4): the right-hand-side residual terms are identical. However, the left hand side terms are different because of the tangent form of Eq. (31).

The reference error equation can be obtained by discretizing Eq. (31). That allows to characterize the reference error  $e_{\tilde{h}}$  as the solution of a linear problem:

$$a_T(u_h; e_{\tilde{h}}, v_{\tilde{h}}) = l(v_{\tilde{h}}) - a(u_h, v_{\tilde{h}}) \text{ for all } v_{\tilde{h}} \in V_{\tilde{h}}, \quad (32)$$

which is analogous to Eq. (7). Although the original problem and, hence, the error equation Eq. (30) are nonlinear, Eq. (32) is a linear system of equations. In fact, the matrix of this linear system of equations, which is associated with the bilinear form  $a_T(u_h; \cdot, \cdot)$ , is the standard tangent matrix. Notice that the tangent matrix (or its approximation) is typically available in finite element codes. the linear system of equations (32) is still unaffordable because of its size. Nevertheless, since Eq. (32) is linear, the linear error estimator presented in section 3 can be fully extended to this nonlinear case. The philosophy of the method is identical: the only difference is that instead of the linear error equation (4), the tangent version of Eq. (31) is employed.

Once interior and patch estimates are computed, they must be measured and added. Thus, in order to completely generalize the linear case, a nonlinear energy norm must be defined. If the tangent form  $a_T(u_h; \cdot, \cdot)$  is symmetric positive definite the reference error  $e_{\tilde{h}}$  computed using Eq. (32) is the projection of the actual error  $e$  on  $V_{\tilde{h}}$  following the scalar product  $a_T(u_h; \cdot, \cdot)$ . Thus, the norm induced by  $a_T(u_h; \cdot, \cdot)$  is taken to measure the error.

**Remark 7** *The norm induced by  $a_T(u_h; \cdot, \cdot)$  is analogous to the linear energy norm defined in Eq. (3) and is also interpreted, from a physical viewpoint, as an energetic quantity. The measure of the error can be understood as the energy needed to move the system from the state described by the approximate solution  $u_h$  to the state associated with the actual solution  $u$ .*

As already remarked, tangent matrices may be computed straightforward, consequently, the tangent versions of the local problems of Eq. (9) and Eq. (15) may be naturally implemented in the finite element code. It is worth noting that, in the patch estimation phase, the orthogonality condition of Eq. (19) must be replaced by its tangent version:

$$a_T(u_h; \eta_l, \varepsilon) = 0 . \quad (33)$$

This linear restriction can also be easily implemented using the Lagrange multiplier technique.

Note that the structure and the rationale of the linear estimator is fully respected and, consequently, the nonlinear generalization inherits all the properties of the linear counterpart.

## 5 Examples

This section shows the application of the presented estimator to a highly nonlinear softening mechanical problem. Perzyna viscoplastic model [23] is used to obtain a regularized softening behavior. The computations account for both material nonlinearity and geometrical nonlinearity. Strain softening is associated with strain localization and, consequently, the use of adaptive techniques to capture the two scales of the problem is practically unavoidable.

In the adaptive processes shown here, the Li and Bettess [20] criterion is used as a remeshing strategy. This criterion is optimal in the sense that minimizes the number of elements in the mesh ensuring that the global error is below a prescribed accuracy. The quadrilateral meshes have been obtained using the mesh generator introduced by Sarrate [25]: the resulting meshes verify the element size prescriptions without having distorted elements.

The influence of pollution errors is discussed in the first example. The pollution errors are expected to become negligible along the remeshing process because the problem is elliptic. In the successive meshes, elements are concentrated in the singularity zones and, consequently, the singularities do not pollute anymore the solution. Thus, as expected, this example shows that taking into account the pollution or not does not make a significant difference in the final results. The second example is used to show the ability of adaptive strategies to capture unexpected solutions (complex failure mechanisms). Both examples reproduce the compression of a plane strain rectangular specimen. In order to induce the strain localization in the specimen, circular openings are introduced, playing the role of imperfections. The difference between the two presented examples is the number and the location of these circular openings. In both examples the tests are driven by imposing the velocity at the top of the specimen.

### 5.1 Example 1: specimen with one centered imperfection

In this example the specimen has one centered circular opening and, consequently, the two axes of symmetry allow to study only one fourth of the specimen, see Figure 5. Figure 6 shows the behavior of the tested specimen: the collapse mechanism is formed by two symmetric strain localization bands

and softening is observed in the macroscopic reaction-displacement curve.

An adaptive procedure has been used. First the computations are carried out with a coarse almost uniform mesh, see mesh 0 in Figure 7. Then the error is estimated at the end of the loading process. Using the estimated error distribution, a remeshing criterion and a mesh generator, a new mesh is created and the computations are carried out from scratch. This is repeated until the estimated error is below some acceptability requirements.

Two series of adapted meshes are presented. In the adaptive procedure of Figure 7 the error is estimated only locally (interior and patch estimate), in the series shown in Figure 8 pollution errors are also taken into account. The goal in both examples is to obtain an error below the 0.5%. Discretizations corresponding to the local estimate have less elements than the ones obtained considering the pollution error. This is because the local error is lower and, consequently, a mesh with less elements suffices. However, the final distributions of elements are very similar. In fact, the pollution error is only relevant in the first mesh which is coarse and roughly uniform. Once the discretization is refined where it is needed (in particular in the vicinity of the singularities) the pollution effects are attenuated and become negligible. This is shown in Figure 9 where the distribution of the index  $r_k$  is plotted. The index  $r_k$ , defined as

$$r_k := \frac{\|e_L\|}{\sqrt{\|e_L\|^2 + \|e_G^*\|^2}},$$

is close to 100% if the influence of the pollution error is negligible. Figure 9 shows how  $r_k$  tends to be uniform and close to 100% along the remeshing process. Thus, considering pollution error does not make a big difference in the final results. This result was expected given the strong ellipticity of the problem [28]. Figure 8 shows also the evolution of the error distribution along the adaptive procedure. The distribution of the error tends to be uniform, as expected. In the sequence of meshes of Figure 8 the prescribed accuracy is attained in mesh 3. It is worth noting that mesh 3 has less elements than the previous one (mesh 2) but also a lower error. In fact, although the remeshing process can be stopped at mesh 3, a further step is carried out to show that the remeshing criterion optimizes the mesh indicating both where the elements must be located and how many elements must be used. Using the information of the error distribution over mesh 3, mesh 4 is built up. Mesh 4 has 8% less elements than mesh 3 but also an acceptable error (under 0.5%). Recall that the remeshing criterion has a goal of 0.5%, thus, in a general sense, mesh 4 proves that the process has converged.

## 5.2 Example 2: specimen with two symmetric imperfections

In this example, the specimen has two circular openings symmetric with respect to the center. That allows to study only one half of the specimen, see Figure 10. Thus, the specimen is divided in two parts by a symmetric line containing the center (the easiest option is to choose a horizontal straight line but many others could be employed). The symmetry conditions prescribe that the nodes on the cut line are homologous with respect to the center point and have opposite displacements. In order to be able to impose these conditions the restriction of the mesh to this cut line must also be symmetric. The number of nodes in each part of this line must be the same and their position must be symmetric: this is an additional restriction for the remeshing procedure that has to be prescribed along the process. Moreover, the nonlinear solvers must be adapted to deal efficiently with these boundary conditions, see [24].

Since the previous example demonstrates that the influence of taking into account pollution errors is negligible, in this example only local estimates are computed.

The mechanism of failure in this case is much more complex than in example 1. In fact, it depends strongly on the position of the circular openings. Two cases are examined with different horizontal gaps between the openings: example 2a and example 2b, see Figure 10.

### **Example 2.a** (*distant openings*)

If the horizontal distance between the circular openings is large enough, the behavior is similar to the previous case. One shear band is developed aligned with the two openings. The remeshing process, see Figure 11, leads to a mesh with a large number of elements concentrated along a single shear band. Figure 12 shows the general behavior of the solution: the softening force-displacement curve is similar to the previous case and the equivalent inelastic strain is concentrated along the shear band, both in the original and the final meshes of the remeshing process. That is, the captured collapse mechanism is the same in both meshes.

### **Example 2.b** (*close openings*)

On the contrary, if the circular openings are closer, the behavior of the solution is much more complex and the original mesh is not able to reproduce such a mechanism.

Figure 13 shows the succession of meshes in this case. It is worth noting that, in the final mesh, according to the concentration of elements, two bands are developed. In fact, the resulting bands are not aligned with the imperfections,



as in example 2.a, but have opposite inclination. Meshes 0 and 1 are not able to reproduce the behavior of the actual solution because the elements in the zone of the second band (which, as shown below, develops in a further stage of the loading process) are too large and, consequently, the model is too stiff. Then, the size of the elements in this zone does not allow the inception of softening. However, the error estimator indicates that the elements must be reduced in the zone of the second band. Thus, once the remeshing process introduces small enough elements along the second band, in meshes 2 to 5, a second mechanism can also be captured. Figure 13 shows also the distribution of the error along the remeshing process, which tends to be uniform, as expected. In the first meshes, the error is larger along the bands and, consequently, the successive discretizations concentrate elements in these zones. Notice that in the final stages the elements are, in fact, concentrated along the edges of the bands, where the gradients of the displacements are large.

The evolution of the meshes in the remeshing sequence of Figure 13 suggest that the actual complex failure mechanism is ignored by the first discretizations and can only be captured using the adapted meshes. This is confirmed comparing the deformation patterns and the force-displacement curves obtained with different meshes.

Figure 14 shows for the final situation (maximum displacements) the computed equivalent inelastic strain and the deformation for different meshes. Only after two remeshing steps the mesh captures two bands. In the previous meshes the discretization is not accurate enough and only one band is completely developed. Since large deformations are considered, once the first band is completely generated, its kinematic mechanism locks; then a second band appears as a new deformation mode with less energy. Figure 15 shows how the force-displacement curves for meshes 0 and 1 of Figure 14 are qualitatively different from meshes 2 to 5. In fact the shapes of the force-displacement curves for meshes 2,3,4 and 5 are practically identical and have two inflections in the descending branch. The solution given by the last mesh is obviously more accurate than the original one because the energy of deformation (area under the force-displacement curve) is lower. In fact, since the error is controlled in energy norm, one can be sure that the actual curve, associated with the exact solution, is not too far from the obtained curve (the error in energy norm is less than 1.5% for the last mesh, thus, the difference of the area under the plotted curve and the exact one would be less than 1.5%).

Thus, this example demonstrates that adaptivity based on error estimation is an essential tool for the determination of a priori unpredictable final solutions. Without this adaptive strategy, the initial mesh (mesh 0 in figure 13) and the resulting solution could be regarded as correct, and the second mechanism would not be detected.

## 6 Concluding remarks

A residual type a posteriori error estimator for nonlinear finite element analysis is introduced. This estimator is a straightforward generalization of a linear residual type estimator. The nonlinear version inherits all the properties of the linear counterpart. Thus, the obtained estimate is a lower bound of the actual error, that is, a systematic underestimation of the error is introduced. However, this underestimation has been found to be small. On the other hand, this estimator can be applied to a wide range of problems discretized by general unstructured meshes, even with different element types. Moreover, the efficiency of the estimator does not depend on superconvergence properties and may include the assessment of the pollution errors with a little supplementary computational effort. The implementation of the estimator in a finite element code is simple because the basic operations are performed by standard routines.

Numerical examples demonstrate the efficiency of the estimator. The adaptive process yields good meshes and equidistributed error. As expected for elliptic problems, the influence of the pollution error tends to be negligible at the end of the remeshing process. Moreover, adaptivity using this estimator allows to capture complex solutions that are ignored by a first mesh. Only the adapted meshes are able to properly describe the complex failure mechanisms.

## References

- [1] Ainsworth, M. and J.T. Oden (1993), “A unified approach to a posteriori error estimation using element residual methods”, *Numerische Mathematik*, **65**, 23–50.
- [2] Babuška, I., R. Durán and R. Rodríguez (1992), “Analysis of the efficiency of an a posteriori error estimator for linear triangular finite elements”, *SIAM Journal of Numerical Analysis*, **29** 947–964
- [3] Babuška, I. and R. Rodríguez, (1993), “The problem of the selection of an a posteriori error indicator based on smoothening techniques”, *International Journal for Numerical Methods in Engineering*, **36** 539–567
- [4] Babuška, I., T. Strouboulis, C.S. Upadhyay and K.S. Gangaraj (1995), “A posteriori estimation and adaptive control of the pollution error in the  $h$ -version of the finite element method”, *International Journal for Numerical Methods in Engineering*, **38** 4207–4235
- [5] Babuška, I., T. Strouboulis, K.S. Gangaraj and C.S. Upadhyay (1997), “Pollution error in the  $h$ -version of the finite element method and the local

- quality of the recovered derivatives” *Computer Methods in Applied Mechanics and Engineering*, **140** 1–37
- [6] Babuška, I., T. Strouboulis and K.S. Gangaraj (1997), “A posteriori estimation of the error in the recovered derivatives of the finite element solution” *Computer Methods in Applied Mechanics and Engineering*, **150** 369–396
- [7] Bank, R.E. and A. Weiser (1985), “Some a posteriori error estimators for elliptic partial differential equations”, *Mathematics of Computation*, **44**, 283–301
- [8] Chow, S.S. & G.F. Carey (1993), “Superconvergence phenomena in nonlinear two-point boundary-value problems”, *Numerical Methods for Partial Differential Equations*, **9** 561–577
- [9] Ciarlet, P.G. (1983) *Introduction à l’analyse matricielle et à l’optimisation*, Masson, Paris
- [10] Cirak, F. and E. Ramm “A-posteriori error estimation and adaptivity for linear elasticity using the reciprocal theorem”, submitted to *Computer Methods in Applied Mechanics and Engineering*
- [11] Díez, P., J.J. Egozcue and A. Huerta, “A posteriori error estimation for standard finite element analysis”, to appear in *Computer Methods in Applied Mechanics and Engineering*
- [12] Díez, P., J.J. Egozcue and A. Huerta (1997), “Analysis of the average efficiency of an error estimator”, In: M. Křížek et al. eds, *Finite Element Methods: Superconvergence, Post-processing and a Posteriori Error Estimates*, Jyväskylä, Finland, 1996 (Marcel Dekker, New York) 113–126
- [13] Díez, P., M. Arroyo and A. Huerta, “Adaptivity based on error estimation for viscoplastic softening materials”, submitted to *Mechanics of Cohesive-Frictional Materials*
- [14] Fourment, L & J.L. Chenot (1995), “Error estimators for viscoplastic materials: application to forming processes”, *Engineering Computations*, **12** 469–490
- [15] Gallimard, L., P. Ladevèze & J.P. Pelle (1996), “Error estimation and adaptivity in elastoplasticity”, *International Journal for Numerical Methods in Engineering*, **39**, 189–217
- [16] Hughes, T.J.R. (1987), *The finite element method*, Prentice Hall International, Stanford
- [17] Ladevèze, P., J.P. Pelle and Ph. Rougeot (1991), “Error estimation and mesh optimization for classical finite elements”, *Engineering Computations*, **8**, 69–80
- [18] Ladevèze, P. and Ph. Rougeot (1997), “New advances on a posteriori error on constitutive relation in f.e. analysis”, *Computer Methods in Applied Mechanics and Engineering*, **150**, 239–249

- [19] Lee, C.Y. & J.T. Oden (1994), “A posteriori error estimation of  $h - p$  finite element approximations of frictional contact problems”, *Computer Methods in Applied Mechanics and Engineering*, **113** 11–45
- [20] Li, L.Y. and P. Bettess (1995), “Notes on mesh optimal criteria in adaptive finite element computations”, *Communications in Numerical Methods in Engineering*, **11**, 911-915.
- [21] Oden, J.T., L. Demkowicz, W. Rachowicz and T.A. Westermann (1989) “Toward a universal h-p adaptive finite element strategy, part 2. A posteriori error estimation”, *Computer Methods in Applied Mechanics and Engineering*, **77**, 113-180
- [22] Ortiz, M. & J.J. Quigley IV (1991), “Adaptive mesh refinement in strain localization problems”, *Computer Methods in Applied Mechanics and Engineering*, **90**, 781–804
- [23] Perzyna, P. (1966), “Fundamental problems in viscoplasticity”, *Recent Advances in Applied Mechanics*, Academic Press, New York, **9**, 243-377.
- [24] Rodríguez-Ferran, A. and A. Huerta, “Adapting Broyden method to handle linear constraints imposed via Lagrange multipliers”, submitted to *International Journal for Numerical Methods in Engineering*
- [25] Sarrate, J. (1996), *Modelización numérica de la interacción fluido-sólido rígido: desarrollo de algoritmos, generación de mallas y adaptividad*, Doctoral Thesis, Universitat Politècnica de Catalunya, Barcelona.
- [26] Strouboulis, T. and K.A. Haque (1992), “Recent experiences with error estimation and adaptivity, Part I: Review of error estimators for scalar elliptic problems”, *Computer Methods in Applied Mechanics and Engineering*, **97**, 399–436
- [27] Strouboulis, T. and K.A. Haque (1992), “Recent experiences with error estimation and adaptivity, Part II: Error estimation for  $h$ -adaptive approximations on grids of triangles and quadrilaterals”, *Computer Methods in Applied Mechanics and Engineering*, **100**, 359–430
- [28] Wahlbin, L.B. (1991), “Local behavior in finite element methods” in P.G. Ciarlet and J.L. Lions (eds.) *Handbook of numerical analysis*, Vol. II, North-Holland, Amsterdam, 357-522
- [29] Yu, J., D. Peric & D.R.J. Owen (1992), “Adaptive finite element analysis of a strain localization problem for the elastoplastic cosserat continuum”, in D.R.J. Owen et al. (eds.), Proceedings of the third international conference on computational plasticity, COMPLAS III, Pineridge Press, Swansea 551–566
- [30] Zhu, J.Z., E. Hinton and O.C. Zienkiewicz (1993), “Mesh enrichment against mesh regeneration using quadrilateral elements”, *Communications in Numerical Methods in Engineering*, **9**, 547-554

- [31] Zhu, J.Z. (1997), “A posteriori error estimation—the relationship between different procedures”, *Computer Methods in Applied Mechanics and Engineering*, **150**, 411-422
- [32] Zienkiewicz, O.C. and J.Z. Zhu (1987), “A simple error estimator and adaptive procedure for practical engineering analysis”, *International Journal for Numerical Methods in Engineering*, **24**, 337-357
- [33] Zienkiewicz, O.C. & G.C. Huang (1990), “A note on localization phenomena and adaptive finite-element analysis in forming processes”, *Communications in Applied Numerical Methods*, **26**, 71–76

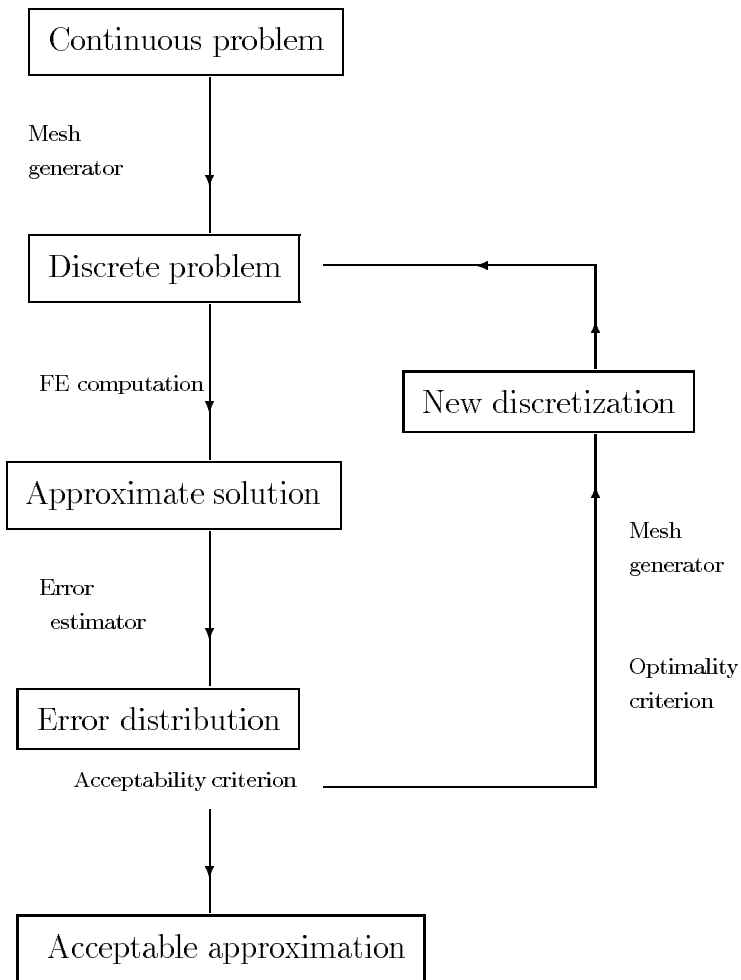
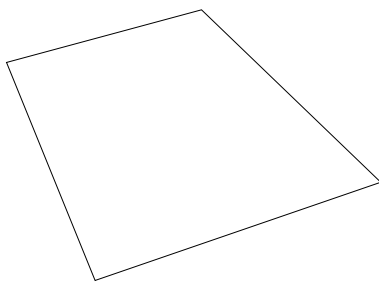


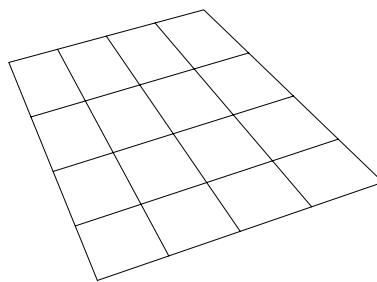
Fig. 1. Flow diagram of an adaptive procedure



(a)



(b)



(c)

Fig. 2. (a), reference submesh mapped into (b), an element, to get (c), an elementary submesh

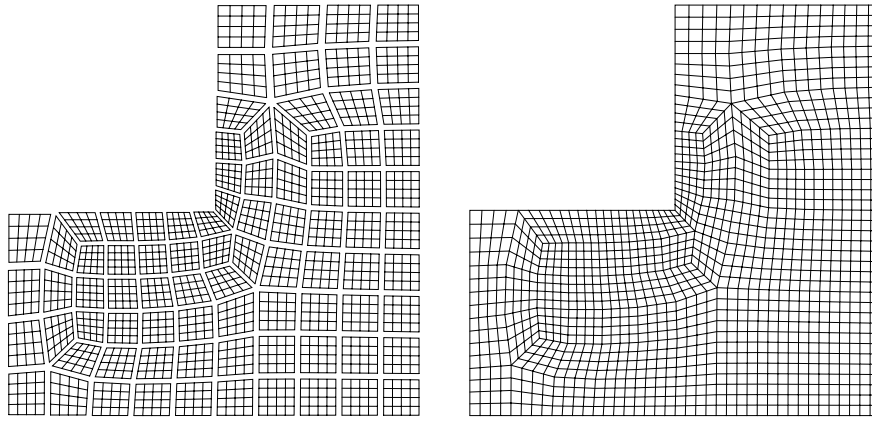


Fig. 3. Set of elementary submeshes and associated reference mesh



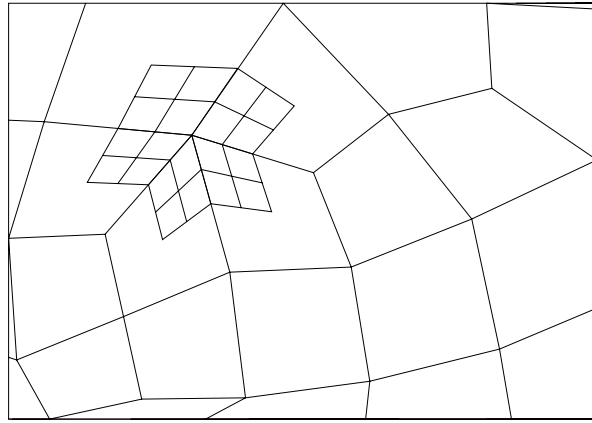


Fig. 4. Patch submesh centered in a node of the computational mesh

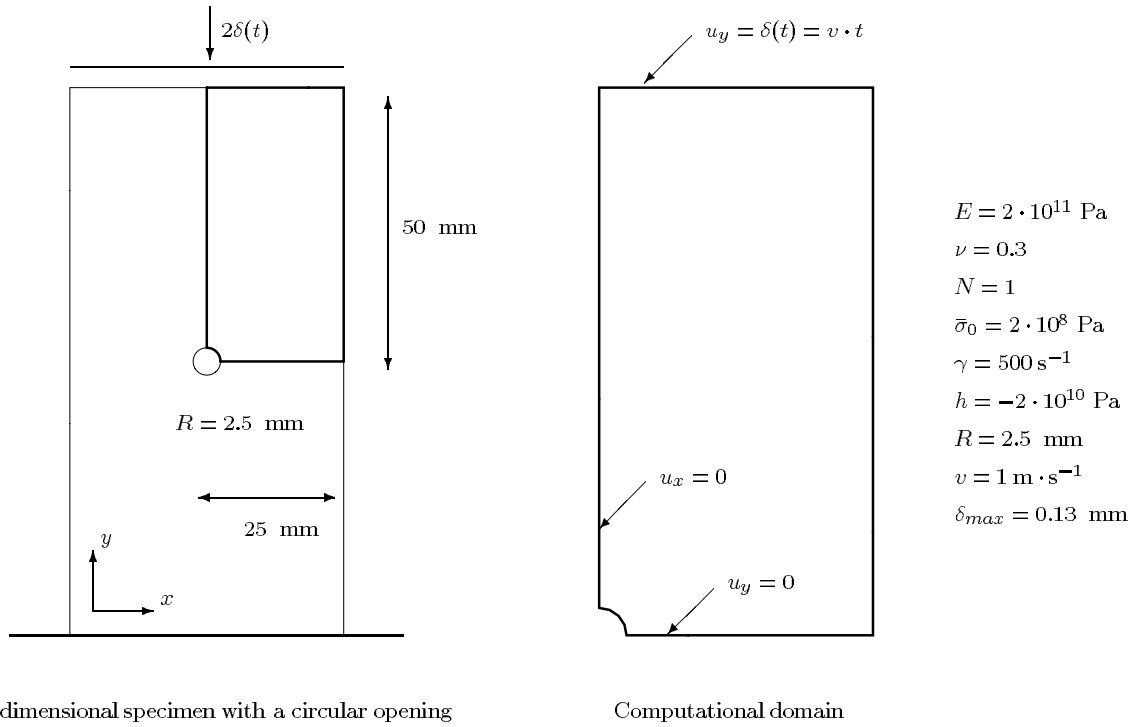
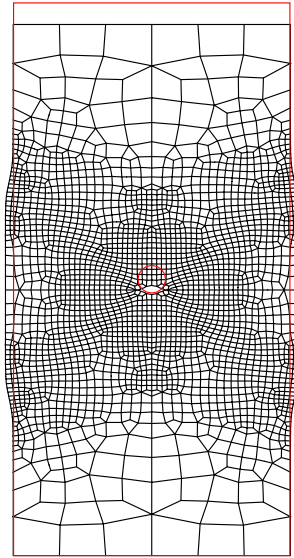
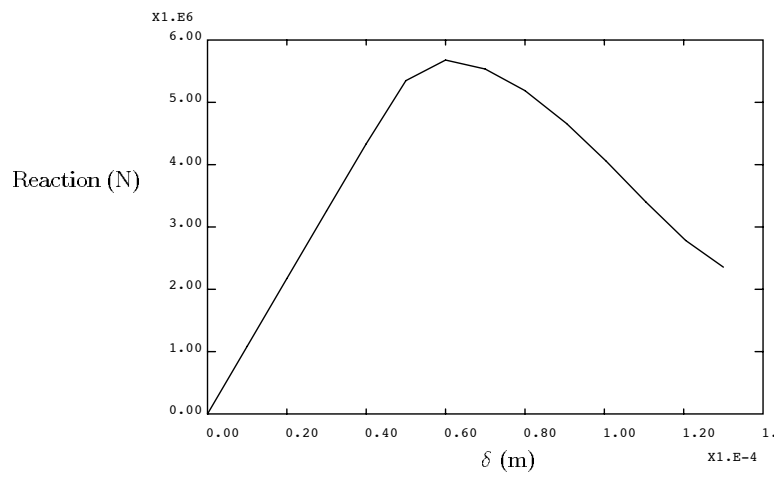
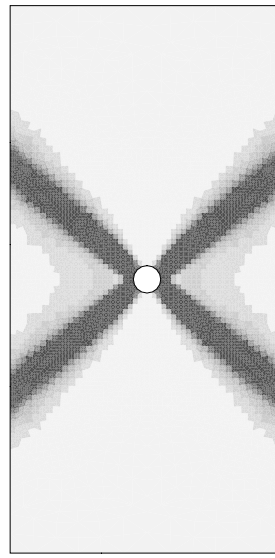


Fig. 5. Rectangular specimen with one centered imperfection



Mesh deformation amplified 15 times



Equivalent inelastic strain

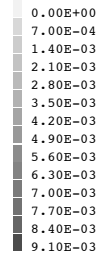
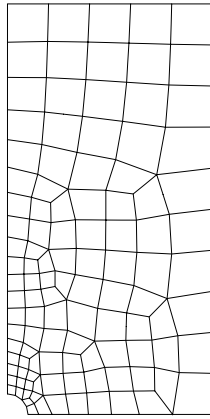
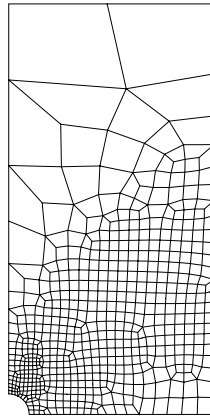


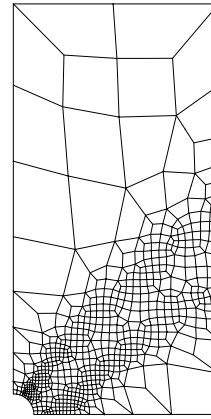
Fig. 6. Description of example 1



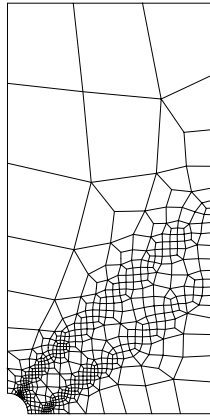
Mesh 0  
110 elements  
Global accuracy: 3.99%



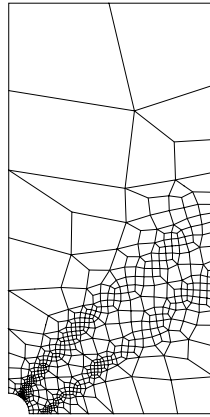
Mesh 1  
550 elements  
Global accuracy: 1.05%



Mesh 2  
611 elements  
Global accuracy: 0.64%

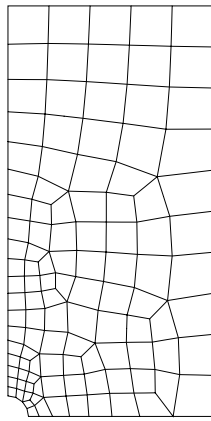


Mesh 3  
561 elements  
Global accuracy: 0.56%

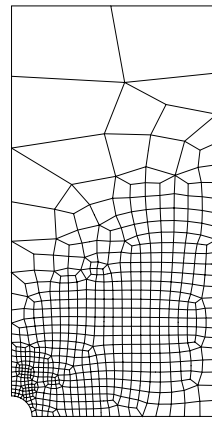
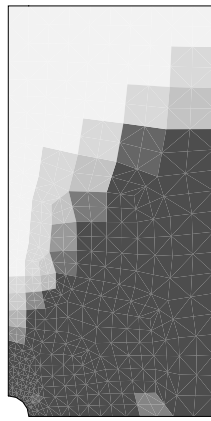


Mesh 4  
564 elements  
Global accuracy: 0.49%

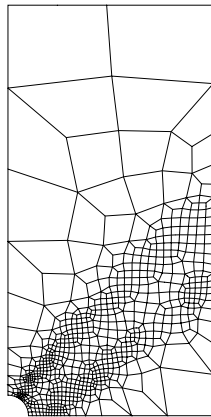
Fig. 7. Remeshing process using Li-Bettess criterion, without pollution errors, for a prescribed accuracy of 0.5%



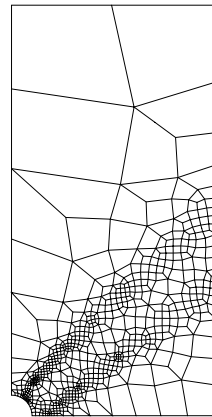
Mesh 0; 110 elements; global accuracy: 4.07%



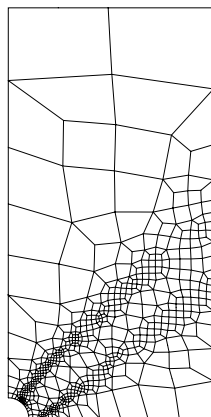
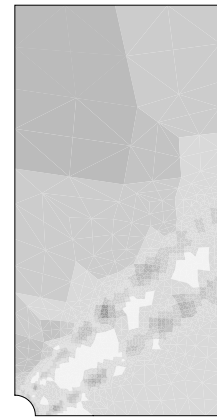
Mesh 1; 580 elements; global accuracy: 1.08%



Mesh 2; 713 elements; global accuracy: 0.56%



Mesh 3; 647 elements; global accuracy: 0.48%



Mesh 4; 601 elements; global accuracy: 0.49%

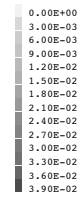
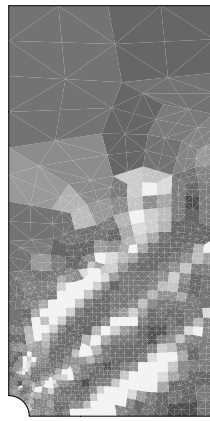


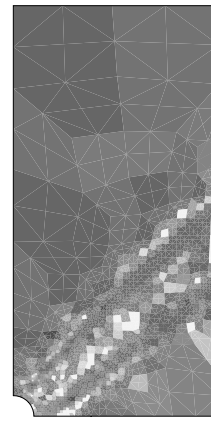
Fig. 8. Remeshing process using Li-Bettess and considering pollution errors for a prescribed accuracy of 0.5%: succession of meshes and estimated error distributions



Mesh 0



Mesh 1



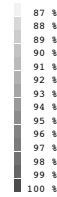
Mesh 2



Mesh 3

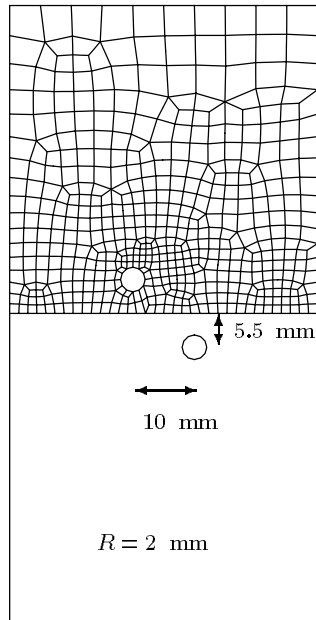


Mesh 4

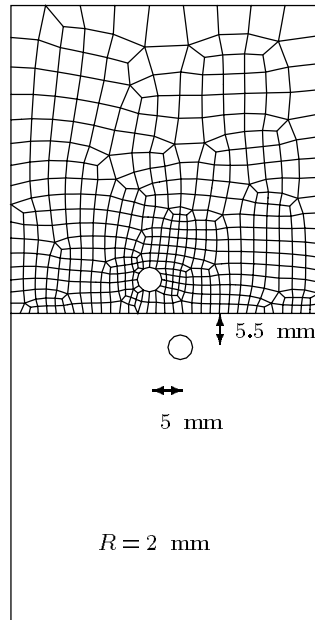


$$r_k := \frac{\|\epsilon_L\|}{\sqrt{\|\epsilon_L\|^2 + \|\epsilon_G^*\|^2}}$$

Fig. 9. Influence of pollution error: distribution of  $r_k$  along the remeshing process accounting for pollution errors

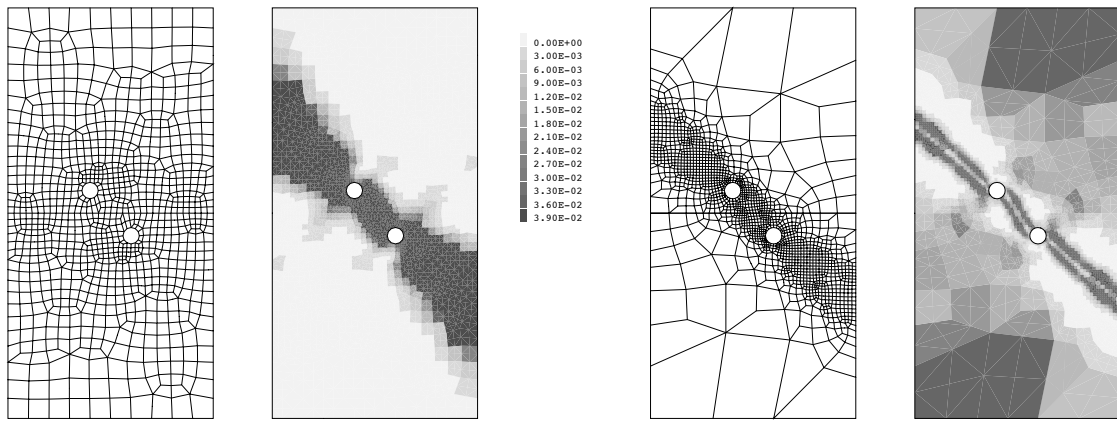


Example 2a: Specimen with two distant circular openings



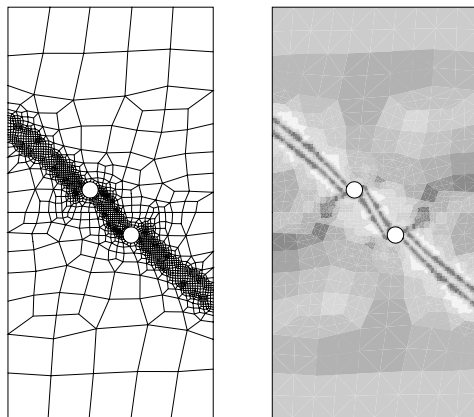
Example 2b: Specimen with two close circular openings

Fig. 10. Rectangular specimen with two symmetric imperfections

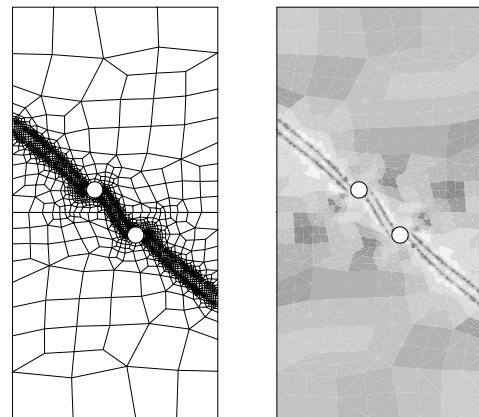


Mesh 0; 470 elements; global accuracy: 6.75%

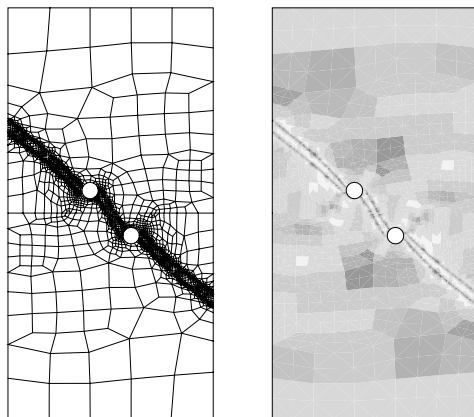
Mesh 1; 781 elements; global accuracy: 3.00%



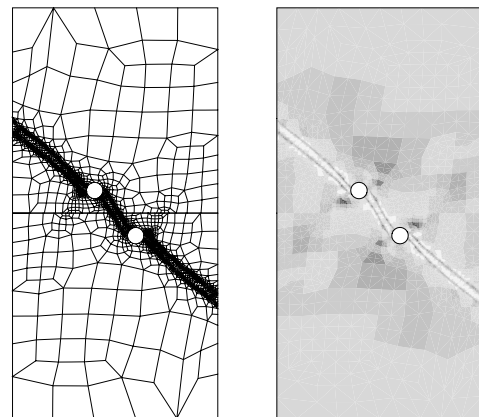
Mesh 2; 899 elements; global accuracy: 2.28%



Mesh 3; 1274 elements; global accuracy: 1.97%

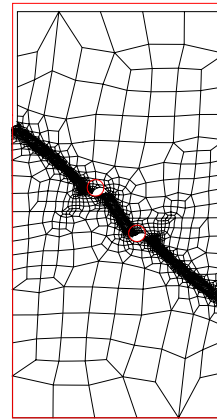
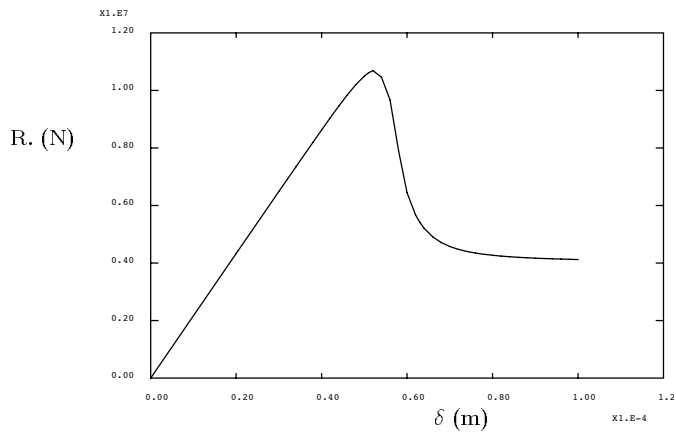


Mesh 4; 1660 elements; global accuracy: 1.62%

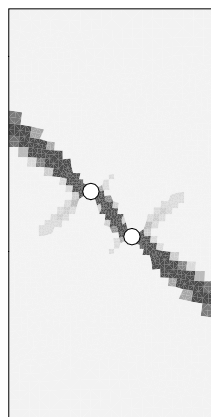


Mesh 5; 1888 elements; global accuracy: 1.35%

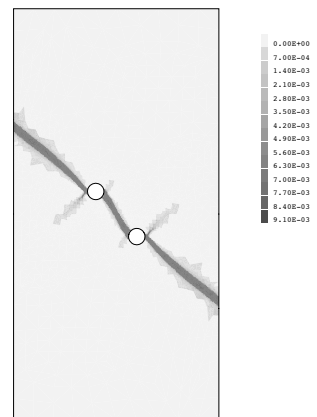
Fig. 11. Remeshing process using Li-Bettess for a prescribed accuracy of 1.5%:  
succession of meshes and estimated error distributions



Mesh deformation amplified 10 times



Equivalent inelastic strain in mesh 0



Equivalent inelastic strain in mesh 5

Fig. 12. General solution for example 2a: Reaction versus imposed displacement, deformation of mesh 5 and inelastic strain contours for meshes 0 and 5



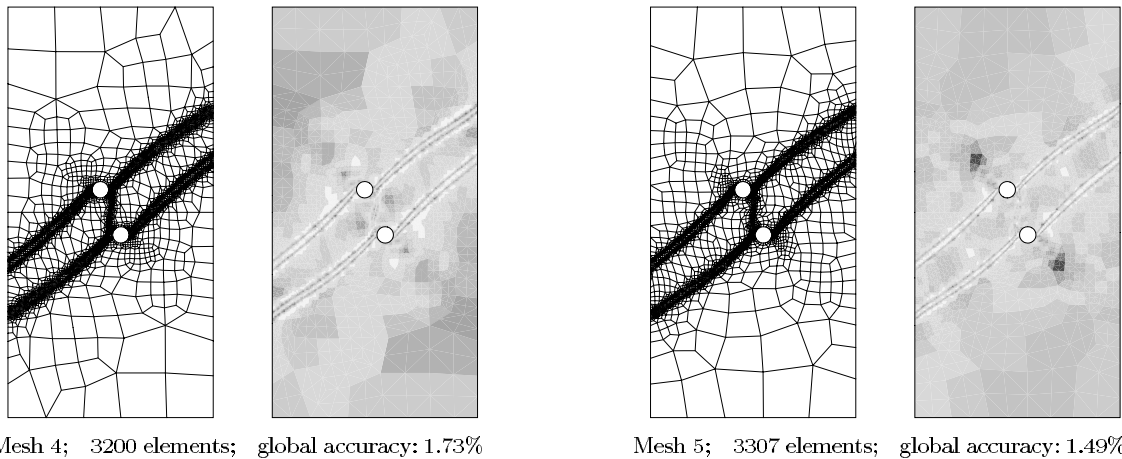
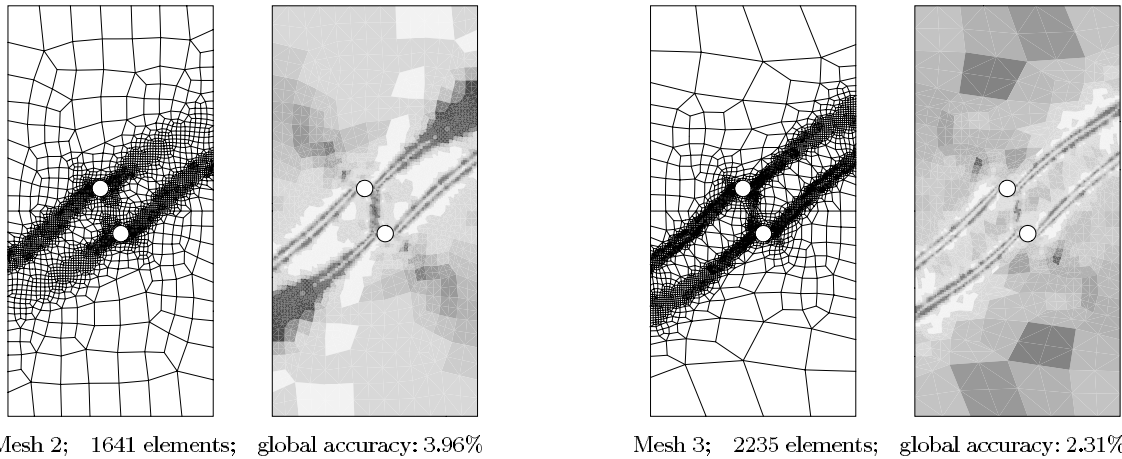
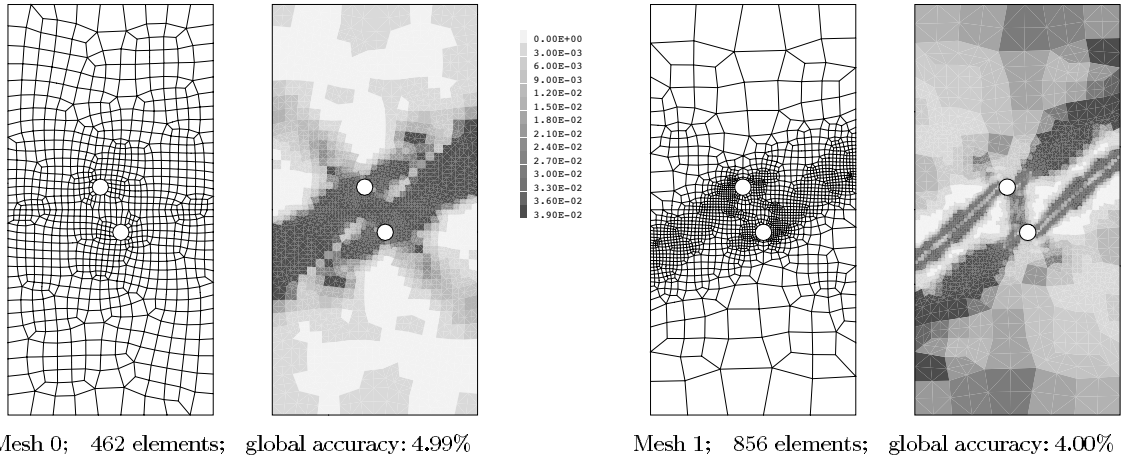


Fig. 13. Remeshing process using Li-Bettess for a prescribed accuracy of 1.5%: succession of meshes and estimated error distributions

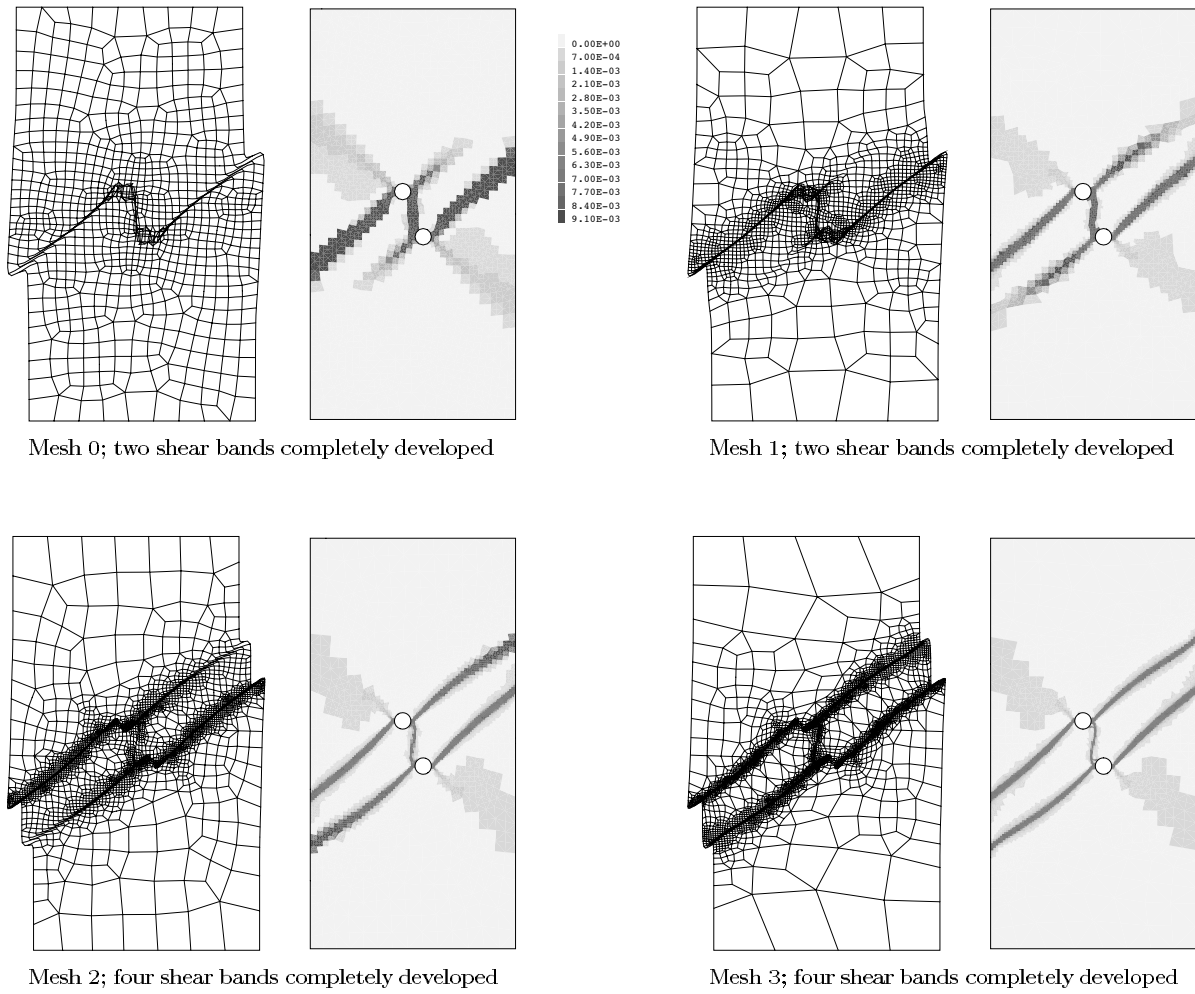


Fig. 14. Deformation amplified 40 times and equivalent inelastic strain contours at the final stage, for meshes 0,1,2 and 3

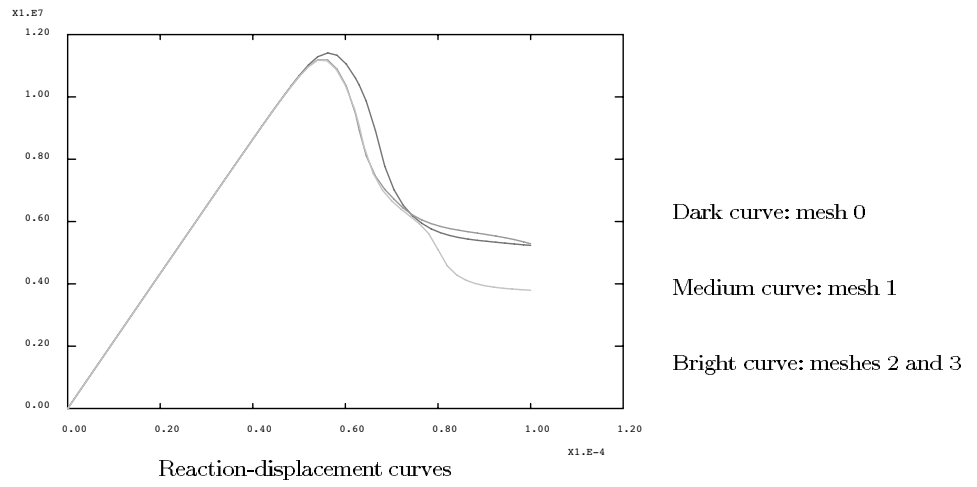


Fig. 15. Force-displacement curves for meshes 0,1,2 and 3

## List of Figures

1	Flow diagram of an adaptive procedure	22
2	(a), reference submesh mapped into (b), an element, to get (c), an elementary submesh	23
3	Set of elementary submeshes and associated reference mesh	24
4	Patch submesh centered in a node of the computational mesh	25
5	Rectangular specimen with one centered imperfection	25
6	Description of example 1	26
7	Remeshing process using Li-Bettesss criterion, without pollution errors, for a prescribed accuracy of 0.5%	27
8	Remeshing process using Li-Bettesss and considering pollution errors for a prescribed accuracy of 0.5%: succession of meshes and estimated error distributions	28
9	Influence of pollution error: distribution of $r_k$ along the remeshing process accounting for pollution errors	29
10	Rectangular specimen with two symmetric imperfections	30
11	Remeshing process using Li-Bettesss for a prescribed accuracy of 1.5%: succession of meshes and estimated error distributions	31
12	General solution for example 2a: Reaction versus imposed displacement, deformation of mesh 5 and inelastic strain contours for meshes 0 and 5	32
13	Remeshing process using Li-Bettesss for a prescribed accuracy of 1.5%: succession of meshes and estimated error distributions	33
14	Deformation amplified 40 times and equivalent inelastic strain contours at the final stage, for meshes 0,1,2 and 3	34
15	Force-displacement curves for meshes 0,1,2 and 3	35